Alveolar Epithelial Cell Differentiation During Lung Repair Requires Cell-Extracellular Matrix Interactions

Jennifer M.S. Sucre[1,4], Fabian Bock[2], Nicholas M. Negretti[1], John T. Benjamin[1], Peter M. Gulleman[1], Xinyu Dong[4], Kimberly T. Ferguson[1], Christopher S. Jetter[1], Wei Han[3], Yang Liu[3], Seunghyi Kook[1], Jason Gokey[3], Susan H. Guttentag[1], Jonathan A. Kropski[3,4,5], Timothy S. Blackwell[3,4,5], Roy Zent[2,4,5], Erin J. Plosa[1*]

[1] Department of Pediatrics, Division of Neonatology, Vanderbilt University Medical Center, Nashville, TN, USA.
[2] Department of Medicine, Division of Nephrology and Hypertension, Vanderbilt University Medical Center, Nashville, TN, USA.
[3] Department of Medicine, Division of Allergy, Pulmonary, and Critical Care Medicine, Vanderbilt University Medical Center, Nashville, TN, USA.
[4] Department of Cell and Developmental Biology, Vanderbilt University Medical Center, Nashville, TN, USA.
[5] Nashville Veterans Affairs Medical Center, Nashville, TN, USA.

* Correspondence:
Erin Plosa, MD
2215 B Garland Ave
1125 Light Hall/ MRB IV
Nashville, TN 37232-0656
+1 615-343-4876
erin.plosa@vumc.org

The authors have declared that no conflict of interest exists.

Abstract

During alveolar repair, cuboidal type 2 alveolar epithelial progenitors rapidly proliferate and differentiate into flat type 1 alveolar epithelial cells. The mechanisms that regulate differentiation after injury may not recapitulate developmental programs as the timing, matrix, and degree of differentiation differs. We previously defined a role for epithelial-matrix interactions in lung organogenesis mediated by integrin extracellular matrix receptors. To test if β1-containing integrins are required during repair, we administered intratracheal lipopolysaccharide to mice with a post-developmental type 2 epithelial β1 deletion. Despite recoverable mild injury in littermate controls, β1-deficient mice repopulated the alveolus with abundant, rounded epithelial cells co-expressing type 2, type 1, and mixed intermediate cell state markers, but failed to differentiate into mature type 1 cells. With differentiation stalled, distal stem cell proliferation persisted with escalation of incompletely differentiated epithelial cells in late repair. These findings demonstrate that β1-containing integrins are exquisitely required for terminal epithelial differentiation post-injury.

Introduction

During lung development, primordial epithelial cells proliferate, migrate, and change phenotypic identity with precise timing, anchored by signals from the basement membrane (BM), a specialized extracellular matrix (ECM) structure, that is precisely remodeled at specific developmental check points (1). Once lung development is complete, targeted replacement of epithelial cells and slow turnover of the alveolar basement membrane protects the alveolar structure during homeostasis in the mature lung. However, epithelial cells lose capacity for efficient proliferation and differentiation as the BM ages (2), increasing susceptibility to chronic lung diseases over time. In contrast to temporally precise development and the relatively quiescent adult lung, repair of acute lung injury must occur rapidly in order to restore a gas-exchanging epithelium to maintain survival. The immediacy of repair results in epithelial proliferation and differentiation that occurs in bulk. For a wild-type mouse, the mild lung injury induced by a single dose of intratracheal lipopolysaccharide (LPS) is easily recoverable in days, overcoming inflammation-derived proteolytic damage to the basement membrane that occurs within hours (3, 4). LPS, as a model of acute inflammatory lung injury, tests the regenerative potential of the alveolus, exposing impairments in epithelial-ECM interactions that could exacerbate lung injury or predispose to accelerated aging.

Integrins are heterodimeric transmembrane protein receptors composed of an α and β subunit that bind ECM ligands. Integrins provide physical connections between cells and the ECM, and they propagate signaling to and from the surrounding matrix (5-7). Of the 24 integrin heterodimers, 12 contain the β1 subunit, and many of the 12 β1-containing integrins are present in epithelial tissues. Integrin function is dependent upon developmental and microenvironmental

context, a concept consistent with our previous work. We previously reported that epithelial β1 integrins are required for normal lung development and in their absence airway branching and alveolarization are impaired, associated with incomplete epithelial differentiation in the later stages of lung development (8). However, in the homeostatic post-developmental adult alveolus, β1 integrins are completely dispensable for alveolar epithelial differentiation (9). Function of the alveolar stem cell niche during repair depends on the rapid proliferation of distal epithelial progenitors, followed by en masse differentiation. The degree of differentiation in this context is profound, and any inefficiencies in this process will create structural vulnerability and abnormal repair. Whether or not β1-containing integrins are required for the epithelial repair cycle in the acutely injured adult alveolus is unknown.

The adult alveolar BM is primarily composed of collagen IV and laminin and facilitates gas exchange between the airspace and the capillary network. The vast majority of the BM is covered with very thin and outspread type 1 alveolar epithelial cells (AT1 cells), interspersed with single cuboidal type 2 alveolar epithelial cells (AT2 cells). Each cell type has essential functions: AT2 cells secrete surfactant to reduce alveolar surface tension, and function in an immunoregulatory role, while the thin AT1 cells allow gas exchange, maintain water homeostasis, and produce BM components (10). Following alveolar injury in both human lung disease and murine models, multiple types of epithelial progenitors restore epithelial coverage of the BM (11, 12). The most proximate and immediate epithelial progenitors for alveolar repair are AT2 cells themselves, a subset of which proliferate upon alveolar injury (13-15). Several pathways drive AT2 progenitor-cell proliferation, including epidermal growth factor receptor pathway (EGFR), insulin-like growth factor receptor (IGFR), fibroblast growth factor pathway,

hepatocyte growth factor (HGF) pathway, wingless/integrated (Wnt) pathway, and yes-associated pathway 1 (YAP) signaling (13, 15-20). Over-proliferation of AT2 cells is restrained by various proteins including the tight junction protein Claudin-18 (20). After proliferation, the AT2 progenitors attain an AT2-to-AT1 transitional cell state with characteristic expression of genes such as *Krt8, Hbegf,* or *Areg* (11, 21, 22), on their way to becoming replacement AT1 cells. Less is understood about the molecular mechanisms that govern the final point of transition in alveolar repair, the acquisition of the AT1 transcriptional phenotype and the full extension of the AT1 outspread cell shape.

Here, we compared distal lung epithelium restoration after acute lung injury induced by intratracheal LPS administration in normal adult mice to those carrying a β1-integrin inactivation targeted to SP-C–expressing AT2 cells. From this modest acute lung injury, β1-deficient mice exhibited increased inflammation and had exacerbated lung injury, followed by emphysema late in repair. Impaired alveolar repair mechanisms in injured β1-deficient mice resulted in excessive AT2 proliferation, progressive accumulation of AT2/AT1 intermediate cells, and large-scale failure of AT1 differentiation. In these studies, the degree of cell-shape block in β1-deficient mice demonstrates that AT2-to-AT1 differentiation is tightly integrated with cell shape change. Further, we show that epithelial differentiation during repair bears a particular requirement for β1 integrin-mediated cell-ECM interactions, more than AT2-to-AT1 differentiation in other contexts. Unlike the assumption that AT2-to-AT1 epithelial differentiation processes employ similar basic mechanistic pathways no matter the context, our data suggest a different paradigm for adult injury repair wherein the rapidity with which differentiation must occur and/or the condition of the ECM leads to distinct differentiation mechanisms.

Results

β1 integrin deletion in AT2 cells increases susceptibility to injury and abnormal repair

To determine the role of epithelial β1 integrin in alveolar repair after injury, we generated mice with a β1-integrin deletion in AT2 cells in the adult lung utilizing the SP-C–rtTA; TetO-Cre doxycycline-inducible system (9, 23) and floxed β1-integrin ($\beta1^{f/f}$), hereafter referred to as $\beta1^{AT2\text{-}KO}$ mice. We previously reported the efficient deletion of β1 integrin in AT2 cells and sustained β1 integrin expression in $\beta1^{f/f}$ littermate control mice (then termed $\beta1^{rtTA}$ mice) and confirmed normal histology in SP-C rtTA; TetO-Cre; $\beta1^{f/f}$ mice not receiving doxycycline at three months of age (9, 23). While doxycycline toxicity has been reported with embryonic administration (24), we observed no overt histologic or biological toxicity from the rtTA system or from doxycycline itself in this post-developmental model (9). After a one-month time period off doxycycline to minimize side effects from possible doxycycline tissue storage, we challenged $\beta1^{AT2\text{-}KO}$ and littermate $\beta1^{f/f}$ controls with a single intratracheal (IT) dose of lipopolysaccharide (LPS) at three months of age (**Figure 1A**). $\beta1^{AT2\text{-}KO}$ mice exhibited decreased survival compared to $\beta1^{f/f}$ control mice (44% survival at 21 days for $\beta1^{AT2\text{-}KO}$ versus 93% for $\beta1^{f/f}$, n=15 $\beta1^{AT2\text{-}KO}$ and 14 $\beta1^{f/f}$ mice, p=0.0051, **Supp. Figure 1A**), with 100% survival for both PBS-treated $\beta1^{AT2\text{-}KO}$ and $\beta1^{f/f}$ mice (data not shown). Three days post-injury, histological examination revealed an expected increase in inflammatory cells in LPS-treated $\beta1^{AT2\text{-}KO}$ and control $\beta1^{f/f}$ lungs and markedly increased edema in $\beta1^{AT2\text{-}KO}$ lungs (**Figure 1A**). LPS-treated $\beta1^{f/f}$ lungs returned to a normal histological appearance by day 7, while edema and inflammation remained prominent in $\beta1^{AT2\text{-}KO}$ lungs, consistent with an exacerbation of acute lung injury. Failed alveolar repair was evident at 21 days in $\beta1^{AT2\text{-}KO}$ mice, whose lungs exhibited a marked increase in airspace size

and septal destruction. Emphysema was quantified by increased mean linear intercept (28.5±0.9 μm in $\beta1^{f/f}$ lungs vs. 40.2±2.8 μm in $\beta1^{AT2\text{-}KO}$ lungs) (**Figure 1B**). To evaluate alveolar barrier function, we measured bronchoalveolar lavage (BAL) fluid protein levels at all time points (**Figure 1C**). $\beta1^{AT2\text{-}KO}$ BAL fluid contained increased protein in the unchallenged state, as well as at 3 and 7 days post-LPS compared to control $\beta1^{f/f}$ BAL fluid. By 21 days post-injury, protein levels were similar in both mouse strains, indicating restoration of alveolar barrier function in $\beta1^{AT2\text{-}KO}$ lungs.

We collected BAL fluid to characterize the inflammatory response to LPS and found no significant differences in immune/ inflammatory cells between $\beta1^{AT2\text{-}KO}$ and $\beta1^{f/f}$ lungs at three days, during the expected peak of inflammation following LPS (25) (**Figure 1D**). However, in $\beta1^{AT2\text{-}KO}$ mice, there was a delayed inflammatory peak at seven days post-injury characterized by persistently increased neutrophils in BAL fluid from $\beta1^{AT2\text{-}KO}$ lungs (**Supp. Figure 1B**). Although the BAL cell count decreased towards baseline at 21 days in $\beta1^{AT2\text{-}KO}$ lungs, increased numbers of macrophages remained at this time point. These findings were confirmed by quantification of immunostaining for the macrophage marker CD68 (**Supp. Figure 1C-E**), and suggest that persistent inflammation in the lungs of β1-deficient mice may contribute to the development of emphysema in this model.

β1-deficient AT2 cells increase in number post-LPS injury

To determine if and how β1-deficient AT2 cells are blocked in contributing to repair, we performed an in-depth histological and transcriptomic examination of alveolar epithelial cells in $\beta1^{AT2\text{-}KO}$ and $\beta1^{f/f}$ lungs. As occasional non-doxycycline-dependent Cre expression (and possible

associated β1-integrin inactivation) in the airway epithelium apart from the alveolar parenchyma has been reported with this inducible system (24), we limited our analysis and conclusions to the alveolar compartment where we previously validated dox-dependent β1 deletion, and deliberately excluded areas containing or adjacent to airway epithelium. Lung sections immunostained for the AT2 marker pro-SP-C and AT1 marker T1α demonstrate accumulation of pro-SP-C+ AT2s in $\beta1^{AT2\text{-}KO}$ lungs by day seven following LPS injury (**Figure 2A**). By day 21, the alveolar septa were lined by abundant pro-SP-C+ AT2s, accompanied by decreased expression of T1α in $\beta1^{AT2\text{-}KO}$ lungs, suggesting loss of AT1s and large expansion of the AT2 population during the alveolar repair period. Despite the inherent difficulties in AT1 quantification by membrane-localized immunostain, we captured the increased imbalance between AT2 cells and AT1 cells in $\beta1^{AT2\text{-}KO}$ lungs by calculating the number of pro-SP-C+ cells as a percentage of total cells. Whereas the percentage of AT2 cells remained stable from day three into late repair in the $\beta1^{f/f}$ lungs, the percentage of pro-SP-C positive AT2 cells progressively increased throughout later repair in $\beta1^{AT2\text{-}KO}$ lungs (**Figure 2B**). Three days after LPS treatment was the only time point at which the percentage of $\beta1^{AT2\text{-}KO}$ AT2 cells was not significantly increased over control lungs, suggesting an inherent vulnerability for AT2 cells in the absence of β1 integrin during the acute injury phase. The increased AT2 number in $\beta1^{AT2\text{-}KO}$ lungs prompted an examination of proliferation and apoptosis. We assessed AT2 proliferation by co-immunostaining lung sections for the proliferation marker Ki67 and pro-SP-C. $\beta1^{AT2\text{-}KO}$ lungs exhibited increased proliferation in pro-SP-C+ AT2 cells at all sampled time points from uninjured lungs to day 21 post-injury, with peak proliferation at day seven (**Figure 2C-D**). Analyzing cell survival by TUNEL assay co-immunostained with pro-SP-C, we identified a small but significant increase in the total number of apoptotic cells per field in $\beta1^{AT2\text{-}KO}$ lungs on

days 7 and 21 after LPS (**Figure 2E-F**), and a relatively minor increase specifically in β1 deficient AT2s on day 21 (**Figure 2G**). This result suggests that continued large-scale epithelial apoptosis was not a major causative factor in the later-stage development of emphysema seen post-injury.

Overabundant AT2s are transcriptionally distinct during repair in β1$^{AT2\text{-}KO}$ mice

To investigate the transcriptional phenotype of β1-deficient epithelial cells that could explain the development of emphysema and other features of abnormal repair in β1$^{AT2\text{-}KO}$ mice, we performed single-cell RNA sequencing (scRNAseq) on unchallenged and LPS-treated β1$^{f/f}$ and β1$^{AT2\text{-}KO}$ lungs, seven days after LPS exposure. From single-cell suspensions from digested whole lung (n= 3-4 mice/ group pooled into a single sample for each condition), we collected CD45-/Ter119- viable cells by fluorescence-activated cell sorting (FACS), thereby excluding immune and red blood cells. We performed scRNAseq using the 10x Genomics platform, and doublet removal, normalization, and scaling led to 2,926 cells being analyzed. Initially, we integrated our dataset with recently published scRNAseq data from LPS injury (12), and we found similar AT2 cell-types present in both datasets (**Supp. Figure 2)**. To further define our epithelial populations throughout alveolar repair, we analyzed our transcripts utilizing the epithelial markers reported by Strunz et al with a label-transfer technique (11). The markers that define this dataset are composed of a variety of epithelial cell states from multiple time points during bleomycin-induced injury-repair (11). In both LPS-treated and uninjured mice, we found all major alveolar epithelial populations in both β1$^{AT2\text{-}KO}$ and β1$^{f/f}$ lungs (**Figure 3A**). Despite AT1 marker depletion in injured β1$^{AT2\text{-}KO}$ lungs by histology, AT1 cells were isolated in low abundance in all four groups, uninjured and LPS-treated β1$^{AT2\text{-}KO}$ and β1$^{f/f}$ lungs, likely due to

cell loss by FACS because of their relatively fragile structure (26). UMAP embedding identified a distinct epithelial population in $\beta1^{AT2\text{-}KO}$ lungs at seven days after injury (**Figure 3B**). Visualizing the UMAPs of the four individual groups, most of the epithelial cells were classified as AT2s or activated-AT2s, a cell state marked by injury-induced genes. In LPS-treated $\beta1^{AT2\text{-}KO}$ lungs, the mixed AT2 and activated-AT2 cells mapped to a transcriptionally distinct cluster compared to the other three groups. Because this distinct $\beta1^{AT2\text{-}KO}$ cluster was comprised of both AT2 and activated-AT2 cells, we combined these populations for further analysis in all four groups. To identify potential β1 integrin-dependent pathways that regulate AT2 to AT1 differentiation during repair, we examined the top differentially expressed genes by Ingenuity Pathway Analysis in the AT2/activated-AT2 group between uninjured and LPS-treated $\beta1^{AT2\text{-}KO}$ or $\beta1^{f/f}$ mice (**Figure 3C-D** and **Supp. Figure 3A-B**). In uninjured mice, the most enriched pathways were an upregulation of the oxidative stress-response pathway in $\beta1^{AT2\text{-}KO}$ AT2/activated-AT2 cells, followed by senescence, JAK/STAT, and IL-6 signaling pathway. All four of these top pathways being relevant to emphysema and lung senescence (27, 28), suggesting baseline conditions that favor accererated aging in these three month-old mice. In LPS-injured lungs, the top eight differentially up-regulated pathways included regulatory signaling networks related to adherens junctions, actin cytoskeleton, and Rho GTPases. Since remodeling of adherens junctions is necessary for elongation of cell shape and Rho GTPases are intermediary signaling effectors between integrins and the actin cytoskeleton, these data suggest that β1 integrin regulates the transition in cell shape during AT1-cell differentiation.

β1 integrin regulates actin expression and RhoA GTPase activation during alveolar repair.

To investigate how β1 integrin regulates the actin cytoskeleton during alveolar repair, we imaged thick 50 μm cryosections detecting F-actin with phalloidin concurrent with pro-SP-C. The injured $\beta1^{f/f}$ pro-SP-C+ AT2 cells formed actin-based protrusions at the areas of their lateral extensions (arrows in **Figure 4A**), a feature shared with differentiating AT2 (to AT1) epithelial progenitors during development (29). In contrast, AT2s in injured $\beta1^{AT2\text{-}KO}$ lungs were larger and rounded with cortical F-actin. Quantifying AT2 cell size by calculating cell area, they were significantly larger in injured $\beta1^{AT2\text{-}KO}$ lungs (66.8±3.0 μm^2) compared to $\beta1^{f/f}$ lungs (48.4±1.8 μm^2) (**Figure 4B**). Since our scRNA-seq data suggested upregulation of actin-cytoskeleton signaling pathways, we next applied a G-actin probe, JLA20, along with F-actin phalloidin and pro-SP-C to study actin remodeling (**Figure 4C**). We found increased G-actin and F-actin in injured $\beta1^{AT2\text{-}KO}$ lungs, with F-actin primarily cortically localized (arrowheads in Fig. 4C) in the $\beta1^{AT2\text{-}KO}$ lungs. We confirmed these increases by calculating the relative fluorescence of the JLA20 and phalloidin probes in pro-SP-C+ cells using corrected total cell fluorescence to normalize fluorescence to total cell area (**Figure 4D**). Because actin remodeling and localization are mediated in part by the cytoskeletal protein ezrin, we immunodetected ezrin in $\beta1^{AT2\text{-}KO}$ and $\beta1^{f/f}$ lungs on day 7 post-injury combined with *Sftpc* RNA *in situ* hybridization to mark AT2 cells. Ezrin was as expected localized to points of lateral cellular protrusion in elongating AT2 cells in control mice (**Figure 4E)**, while being much more widespread along the cell membrane in AT2s in $\beta1^{AT2\text{-}KO}$ lungs, suggesting an impaired ability to direct actin localization in concert with loss of lateral elongation. We validated the linkage to small GTPases (30) suggested by scRNAseq analysis above using protein assays for specific GTPases. AT2 cells from LPS-injured $\beta1^{AT2\text{-}KO}$ lungs exhibited increased RhoA and Cdc42 GTPase activation, as would be anticipated for a cell undergoing efficient actin remodeling (**Figure 4F-G**). In contrast, GTPase

activation was decreased for Rac1 (**Figure 4H**), a related GTPase involved in forming smaller actin-based structures such as microvilli. Taken together, these data indicate RhoA and Cdc42 GTPase activation in AT2 cells is enhanced in β1 integrin-deficient AT2 cells, as would be expected for a cell with active actin remodeling, but evidence of actin remodeling at the site of lateral extension is absent, suggesting a post-signaling block in $\beta1^{AT2\text{-}KO}$ lungs. Thus, β1 integrin is a critical component for proper actin production and localization in differentiating AT2 cells during repair.

Post-injury β1-deficient AT2s exhibit an AT2-AT1 mixed transcriptomic phenotype

Our histology-based conclusion of increased AT2 cells and decreased AT1 markers (Fig. 2A) suggested significant impairment in AT2 to AT1 differentiation during alveolar repair. To define this defect at the transcriptional level we scored the percentages of lung epithelial cell types as previously defined by Strunz et al (11). Consistent with our histology of the LPS-injured mice (Fig. 2A), there was a significant increase in the representation of AT2 and activated AT2 cells in day seven post-LPS-injury $\beta1^{AT2\text{-}KO}$ lungs, but not control $\beta1^{f/f}$ (**Figure 5A**). We next compared the AT2, AT1, and keratin 8–positive "intermediate cell" transcriptomic profiles in our uninjured and LPS-treated $\beta1^{AT2\text{-}KO}$ and $\beta1^{f/f}$ lungs. Strunz et al. (9) defined intermediate cells, a cell state between AT2 and AT1 cells, found during alveolar repair as "Krt8-positive ADI" (alveolar differentiation intermediate) with both AT1 and AT2 features. Both uninjured and LPS-treated $\beta1^{AT2\text{-}KO}$ and $\beta1^{f/f}$ AT2/activated-AT2 cells expressed typical AT2 markers, *Sftpc, Sftpa1,* and *Abca3*, as expected (**Figure 5B**). The Krt8+ ADI markers *Krt8, Hbegf,* and *Areg* were moderately increased in uninjured β1 lungs and this increase was accentuated post-LPS. There was minimal expression of these markers in uninjured or LPS-treated $\beta1^{f/f}$ lungs. Finally,

uninjured $\beta1^{AT2\text{-}KO}$ AT2/ activated AT2 cells exhibited enhanced AT1-cell marker expression compared to uninjured $\beta1^{f/f}$ AT2 cells, which was also accentuated post-LPS. In summary, absence of β1 increases the proportional representation of intermediate cell states even in cells that remain classified as AT2 cells, indicating a significant block in the progression of the differentiation process.

We next assessed the spectrum of Strunz et al alveolar epithelial markers in those cells classified as Krt8+ ADI cells from uninjured and LPS-treated $\beta1^{AT2\text{-}KO}$ and $\beta1^{f/f}$ lungs (**Figure 5C**). As anticipated, the Krt8+ ADI population strongly expresses one or more of the Strunz et al Krt8+ ADI marker genes, *Krt8, Hbegf,* and *Areg*, in all four conditions. Notably, the Krt8+ ADI populations from both injured $\beta1^{AT2\text{-}KO}$ and $\beta1^{f/f}$ lungs expressed some AT1 markers, consistent with cells attempting transition towards an AT1 cell transcriptional phenotype. Importantly, the $\beta1^{AT2\text{-}KO}$ Krt8+ ADI populations intensely expressed AT2 markers *Sftpc*, *Sftpa1,* and *Abca3*, in both the uninjured and LPS-treated conditions. In contrast, there is only scant expression of these markers retained in Krt8+ ADI cells from $\beta1^{f/f}$ lungs. The retention of AT2 markers in $\beta1^{AT2\text{-}KO}$ Krt8+ ADI cells represents a programmatic delay in differentiation compared to $\beta1^{f/f}$ Krt8+ ADI cells. The continued expression of *Sftpc* in both $\beta1^{AT2\text{-}KO}$ AT2 and Krt8+ ADI cells after injury suggests that requisite β1 integrin-dependent mechanisms, such as cell shape change, preceed and govern the loss of AT2 markers and the acquisition of AT1 markers during alveolar repair.

Mixed-phenotype AT2 cells persist, proliferate, and maintain an enlarged, rounded cell shape in late alveolar repair

Since our histological and scRNA-seq analysis showed impaired AT2 differentiation at day 7 post-LPS, we characterized the blockage in differentiation in late repair. As described above (Fig. 3B), we performed scRNA-sequencing on uninjured and LPS-treated $\beta1^{f/f}$ and $\beta1^{AT2\text{-}KO}$ lungs, 21 days post-LPS. Knowing that alveolar epithelial cells of mixed transcriptomic phenotype exist at day 7 post-LPS in $\beta1^{AT2\text{-}KO}$ lungs, we enhanced our ability to detect differences in persistent incomplete differentiation at day 21 by sequencing CD45-/Ter119- single-cell suspensions enriched for CD326+ epithelial cells. UMAP embedding with label transfer from Strunz et al. revealed similarities between $\beta1^{f/f}$ and $\beta1^{AT2\text{-}KO}$ alveolar cells (**Figure 6A-B**). By pro-SP-C/ Ki67 co-immunostaining, we demonstrated still-increased AT2 proliferation even during late repair (Fig. 2D). Our scRNA-seq data confirmed that the AT2 population from day 21 LPS-treated $\beta1^{AT2\text{-}KO}$ lungs exhibited an increased G2M proliferation score compared to AT2 cells from day 21 LPS-treated $\beta1^{f/f}$ lungs (**Figure 6C**). Similar to the scRNA-seq data from day 7, we next analyzed the expression of AT2, Krt8+ ADI, and AT1 markers in day 21 LPS-treated $\beta1^{AT2\text{-}KO}$ and $\beta1^{f/f}$ alveolar epithelial cells. We identified enhanced AT2 markers, *Sftpc*, *Sftpa1,* and *Abca3*, in AT2 and activated AT2 cell populations from $\beta1^{AT2\text{-}KO}$ mice compared to $\beta1^{f/f}$ mice (**Figure 6D**). In addition, $\beta1^{AT2\text{-}KO}$ Krt8+ ADI cells retained AT2 marker expression compared to $\beta1^{f/f}$ Krt8+ ADI cells, exhibited markedly enhanced expression of the three intermediate state markers (*Krt8, Hbegf,* and *Areg*), and increased expression of AT1 markers, *Aqp5* and *Ager*. These $\beta1^{AT2\text{-}KO}$ Krt8+ ADI cells simultaneously expressed transcriptional markers from all three stages of transition, providing a transcriptional rationale for failed repair in β1-deficient mice. We validated the persistent mixed transcriptional phenotype in $\beta1^{AT2\text{-}KO}$ lungs by immunodetection. In day 21 LPS-treated $\beta1^{AT2\text{-}KO}$ lungs, markedly remodeled areas exhibited numerous pro-SP-C+/ cytokeratin 8+ cells, with

occasional rounded cells that were also positive for the AT1 marker Ager (arrow in **Figure 6E**). Given the disparate cellular morphology of β1-deficient AT2 cells at earlier time points, we quantified differences in cell area in pro-SP-C+ AT2 cells. At 21 days after LPS, injured AT2 cells from $\beta1^{AT2\text{-}KO}$ lungs remained enlarged with a significantly increased cell area (**Figure 6F**). Since lateral extension is necessary for cells to transition from AT2 to AT1 and we demonstrated that cell shape is β1-dependent in AT2 cells, we calculated a roundness score, which quantifies the degree of smooth cellular contours in an unbiased manner. Round cells possess a score closer to 1 and cells with prominent lateral extensions have a lower score towards 0 (31). The roundness score in $\beta1^{f/f}$ AT2 cells transiently decreased at day 3 and day 7, as they differentiated and changed shape into flattened AT1 cells. In contrast, AT2 cells from LPS-treated $\beta1^{AT2\text{-}KO}$ lungs maintained an elevated roundness score throughout repair, consistent with an inability to form lateral extensions and impaired actin remodeling (**Figure 6G**). In summary, these findings demonstrate that β1-mediated ECM interactions are essential during alveolar repair for regulation of AT2 progenitor cell proliferation and organization of requisite cell shape changes that preceed complete transcriptomic differentiation.

Discussion

β1 integrin is exquisitely required for differentiation during repair, in contrast to development or alveolar homeostasis.

Since progenitor AT2 proliferation precedes differentiation in the injury-repair cycle, the overabundance of incompletely differentiated AT2 cells reveals a substantial block in differentiation post-injury. The degree of AT2 accumulation in β1-deficient repair far exceeds the more modest increase in AT2 numbers in mice with a developmental β1 deletion, where AT2 cell numbers in β1-deficient mice are double compared to controls (8). The AT2 cell increase is even more incremental in mice with an adult β1 deletion in the absence of injury, just 60% above control (9). This relative difference in AT2 surplus, coupled with successful AT2 to AT1 differentiation in uninjured aged $\beta1^{AT2\text{-}KO}$ mice (9), shows that β1-ECM interactions are more critical for differentiation during acute repair of adult injury than during development or homeostasis. This comparison suggests β1-dependent differentiation mechanisms are specifically adjusted to fit the requirements of the peripheral stem-cell niche. One possible explanation is that the time interval over which cells change shape and differentiate differs between the three contexts of development, homeostasis, and repair. Developmental AT2 to AT1 differentiation occurs over weeks, and sporadic AT2 replacement of AT1 cells in the adult lung occurs without the urgency of replacing a widely denuded BM. In contrast, AT2 differentiation post-LPS happens en masse with the BM exposed within hours and repopulated within days. This shorter time interval makes robust upregulation of facultative differentiation pathways less likely, exposing a dependence on β1-mediated mechanisms for regulating differentiation. Another possible reason for the β1 requirement during repair may be related to the condition of the BM. It is well known that changes in the relative amounts of ECM components will push the alveolar

epithelium towards proliferation or differentiation (32), although less is known about how structural changes to the BM itself drives epithelial behavior in the alveolar stem cell niche. In lung organogenesis, the BM composition switches at developmentally precise time points, guiding epithelial behavior spatially and temporally as dictated by the developmental program, as reviewed in (1, 33). The mature uninjured lung has a relatively stable BM with slow turnover of BM proteins (34). However, during LPS-induced injury, inflammatory-cell–associated proteases partially degrade the alveolar BM within hours (3, 4, 35). Numerous proteases degrade ECM components preferentially, thereby significantly modifying the carefully balanced alveolar BM composition (4). As different injuries induce varying types of protease-release, damage to the BM components will change depending on type and severity of insult, further shifting β1-ECM interactions in the stem-cell niche away from homeostatic conditions. In addition, individual β1-containing integrin pairs preferentially bind their preferred ECM ligands, thereby setting up a situation where injury-induced changes to β1-ECM interactions can either restrict or augment epithelial differentiation.

The progressive increase in AT2 cell number that escalates late in repair in $\beta1^{AT2\text{-}KO}$ lungs indicates that β1-ECM interactions may serve as a brake on AT2 progenitor cell proliferation, could be a requisite step for progression from proliferation to differentiation during the alveolar injury repair cycle, and that this stalled differentiation stimulates a feed forward loop that creates a continued abnormal call for progenitor proliferation. The lung is unique among branched organs in that there exists a distal (in fact, intra-alveolar) epithelial progenitor representing an indigenous contributor to tissue regeneration (13-15, 36), whereas no such epithelial progenitor has been reported for the kidney, mammary gland, or pancreas. Multiple

signaling pathways have been proposed as positive and negative regulators of AT2 progenitor proliferation in the adult lung, including EGF, IGF, FGF, HGF, Wnt, and Yap-Taz pathways (13-17, 19, 20, 37), but the molecular mechanisms whereby β1 integrin interacts with each of these pathways in the lung remains largely undefined. In other organs, β1-containing integrins have been reported to negatively regulate epithelial proliferation, with an EGFR-activation dependent mechanism identified in the intestinal epithelium (38), but these studies do not consider progenitor proliferation in the context of repair. Consideration of our data in light of this published work suggests that β1 integrin restricts proliferative potential in progenitor AT2s in the injured distal lung.

Failed differentiation in injured β1-deficient mice reveals that cell shape change is intimately tied to progression of differentiation.

We demonstrate that β1-ECM interactions are a requisite component for epithelial cell shape change through regulation of actin remodeling in the injured alveolus. The connection between integrins and regulation of cellular extension comes from studies in Drosophila epithelium and murine podocytes, both in the *uninjured* state (39-43). Our scRNA-sequencing analysis supports the concept that cell shape change is linked to progression of differentiation, as actin remodeling pathways were enhanced in LPS-treated β1-deficient AT2 cells, but differentiation remained blocked with an overabundance of large, rounded AT2 cells. It is possible that loss of integrin clustering at the cell membrane disrupts the spatial specificity of Rho-GTPase signaling (44). Certainly, diffuse ezrin expression associated with persistence of a rounded cell shape and loss of lateral cellular extensions observed in LPS-treated $\beta1^{AT2\text{-}KO}$ AT2 cells is consistent with impaired actin nucleation.

Historically, cellular identity has been defined by histological shape and directly observable characteristics of function (e.g., lamellar body synthesis by electron microscopy). The advent of single-cell transcriptomics increases the granularity with which we can group similar cells together. While this advance augments our understanding of cellular transitional states, the question of how to define groups of similar cells and the boundary between different cell identities is perhaps murkier. Previously published injury models report similar temporary and resolvable transitional cell states after bleomycin injury and other inflammatory stimuli (21, 22), which are marked by high *Krt8* expression. Our transcriptomic data demonstrated persistently blocked AT2-to-AT1 differentiation in injured $\beta1^{AT2\text{-}KO}$ lungs, suggesting that they are stuck in a transitional state even in late repair. Although our model is unique in the degree and persistence of failed differentiation, our transcriptomic data has some similarities and differences with recently published single-cell sequencing data from LPS injury (12). The observed differences in the transitional cell-state populations identified are possibly linked to technical differences in how epithelial cells were sorted; Riemondy et al. used AT2 cells selected by expression of a fluorescent reporter for *Sftpc*-expression prior to scRNAseq, removing transitional cells with lower *Sftpc* expression.

Loss of β1-mediated epithelial-ECM interactions increases susceptibility for emphysematous abnormal repair and accelerates aging.

Loss of β1 integrin in AT2 cells generates a senescent transcriptional signature in an otherwise uninjured youthful lung that translates into emphysematous abnormal repair with injury. Emphysema is a principal component of chronic obstructive pulmonary disease (COPD), one of the most common human pulmonary diseases that increases in incidence with age (45,

46). Although airspace expansion has been reported with either two-hit injury models or chronic repetitive low-dose LPS exposure (47-51), our β1-deficient mice are the first targeted epithelial deletion that results in subacute alveolar destruction following a single LPS exposure, underscoring the importance of epithelial β1 integrin in senescence and its associated pulmonary pathologies. Our scRNA-sequencing pathway analysis demonstrates uninjured β1-deficient AT2 cells possess an inherent susceptibility to injury, as uninjured $\beta1^{AT2\text{-}KO}$ mice exhibit upregulation of oxidative stress, senescence, and inflammatory pathways, all contributing factors to emphysema pathogenesis. LPS-challenged $\beta1^{AT2\text{-}KO}$ mice also exhibit increased inflammation during repair, an associated finding in COPD (52), with a sustained increase in neutrophils at day 7 after LPS, potentially making prolonged exposure to elastase a contributing factor for emphysema development. At 21 days post-injury, $\beta1^{AT2\text{-}KO}$ lungs retain elevated numbers of macrophages, a significant source of matrix metalloproteinase-9 (MMP-9), which remodels alveolar matrix in COPD (49). It is unlikely that increased AT2 apoptosis in $\beta1^{AT2\text{-}KO}$ lungs is the primary mechanism for the development of emphysema as it was only present late in repair at day 21, when emphysematous structural changes had already occurred. The etiology for emphysematous alveolar remodeling in young β1 deficient mice is likely multi-factorial, but rooted in the preexisting upregulation of senescence, oxidative stress, and inflammatory pathways. Additional studies addressing how β1 integrin regulates these pathways would ellucidate if and how β1-dependent mechanisms could increase susceptibililty of human COPD.

In conclusion, this study shows that β1 integrin-mediated mechanisms are a requisite component of rapid and complete alveolar repair following even mild LPS-induced lung injury, and involve regulation of AT2 proliferation, differentiation, and cell-shape change. In the latter,

we propose that cytoarchitectural changes, such as the formation of actin-rich lateral cellular extensions, are specifically tied to progression of AT2 to AT1 differentiation during repair. Loss of β1 integrin results in upregulation of senescence, oxidative stress and inflammatory pathways already pre-injury, thereby increasing susceptibility to emphysema, a common age-related lung structural deficit.

Methods

Mice and LPS injury: We induced β1 integrin in AT2 cells in the adult murine lung by crossing transgenic mice with inducible Cre recombinase expression by the doxycycline-inducible reverse tetracycline transactivator under control of the SP-C promoter (SP-C rtTA; Tet-O-Cre) with integrin $\beta1^{flox/flox}$ ($\beta1^{f/f}$) mice (53, 54). Littermate rtTA negative; Tet-O-Cre negative ($\beta1^{f/f}$ mice were used as control mice. Doxycycline drinking water (2 g/L) was administered for 4 weeks beginning at P28 to triple transgenic SP-C rtTA; Tet-O-Cre; $\beta1^{f/f}$ mice (called $\beta1^{AT2\text{-}KO}$ mice) and littermate $\beta1^{f/f}$ controls, as previously described (9). Following proposed guidelines to limit Cre leak with the doxycycline-inducible system (24), we used the more faithful line 2 strain, employed a breeding strategy to keep the rtTA allele hemizygous, and utilized an injury model that targets the peripheral lung rather than the airway epithelium. After a 1-month period off doxycycline to minimize any potential toxicity from tissue stored doxycycline, we challenged 3-month-old $\beta1^{AT2\text{-}KO}$ and $\beta1^{f/f}$ mice with a single intratracheal dose of LPS or PBS (3 μg/g mouse weight, equivalent volume for PBS) and harvested tissue at the indicated dates. SP-C rtTA and Tet-O-Cre mice were purchased from Jackson Laboratory. Integrin $\beta1^{f/f}$ mice were generously gifted by Elaine Fuchs (Howard Hughes Medical Institute, The Rockefeller University, New York, NY). All mice were maintained on the C57BL/6 background.

Histology and morphological analysis: For histological analysis on paraffin sections, mice were sacrificed, right ventricle was flushed with PBS, and lungs were inflation fixed at 25 cm with 10% formalin. After paraffin processing, embedding and sectioning, lungs were hematoxylin and eosin stained for morphological analysis by mean linear intercept, which was calculated from images (≥ 10 non-overlapping images per mouse) obtained using a x40 objective on a Keyence

BZ-X710 inverted fluorescence phase contrast microscope. Immunofluorescence staining was performed on paraffin or frozen sections, as indicated. Frozen blocks were prepared from lung sections inflation fixed with a 2:1 PBS/O.C.T. (Tissue-Tek) mixture, embedded, and sectioned at either 8 μm or 50 μm thickness. Frozen section slides were then fixed with 4% paraformaldehyde, permeabilized with .1% Triton-X, and blocked with 5% donkey serum for 2 hours at 37 degrees. Slides were incubated in primary antibody overnight at 4 degrees, followed by secondary antibody incubation for 2 hours at room temperature. For sequential primary antibody staining, a second intervening blocking step was utilized. Nuclei were stained with Dapi, ProLong Gold mountant was applied, and imaged. High power images were obtained using a Nikon Spinning Disk TiE inverted fluorescent confocal microscope attached to an Andor DU-897 EMCCD camera (x100 objective, 8 μm sections). All other images were obtained using the Keyence BZ-X710 microscope as above. The following primary antibodies and probes were used: anti-pro-SP-C (Abcam ab90716), anti-T1α (podoplanin, Developmental Studies Hybridoma Bank 8.1.1), anti-ezrin (Cell Signaling Technologies 3145S), anti-cytokeratin 8 (Invitrogen PA5-24607), and anti-Ki67-FITC (eBioscience 11-5698-90), anti-CD68 (Abcam ab125212), anti-Ager (R and D AF1145), JLA20 (Developmental Studies Hybridoma Bank JLA20-s), and phalloidin (Invitrogen A12380). We applied the following secondary antibodies: anti-rabbit Alexa Fluor 594 (Life Technologies A21207), anti-hamster Alexa Fluor 488 (Life Technologies A21110), anti-rabbit Alexa Fluor 488 (Life Technologies A21206), and anti-rabbit Alexa Fluor 647 (Life Technologies A32795). TUNEL staining was performed on paraffin sections co-immunostained with pro-SP-C, per manufacturer's kit instructions (Roche 11684795910). RNA *in situ* hybridization for mouse *Sftpc* was used in conjunction with immunofluorescent staining for the anti-ezrin antibody. RNA *in situ* hybridization was

performed per manufacturer's instructions (RNAScope, ACDBio), including positive and negative control probes. Quantification of immunostained sections was performed on ≥ 10 nonoverlapping images obtained with a 40x objective. JLA20 and phalloidin probe detection was quantified on lung sections (10 sections/ mouse) imaged with equivalent settings using the corrected total cell fluorescence feature from ImageJ, which corrects fluorescence integrated density for the area of the region of interest (pro-SPC+ cells).

Cell morphometry: AT2 cell area and roundness were calculated using the shape descriptor feature of ImageJ with pro-SP-C used to define the region of interest.

Bronchoalveolar lavage: After sacrifice, lungs were lavaged with 1 ml sterile PBS. The cells present in lavage fluid were collected by centrifugation, resuspended, and counted. Protein content in lavage fluid was measured by BCA protein assay (Pierce cat #23225) per manufacturer's instructions.

AEC isolation and GLISA assay: Primary AT2 cells were collected at indicated time points as previously described (8, 9), which yields > 90% AT2s (55, 56). Briefly, single cell lung suspension was generated after dispase digestion and serial filtration. Cells were then applied to plates coated with CD-32 and CD-45 for negative selection. Epithelial cells were then collected from medium after a 2 hour incubation. Cell lysates were then used for G-LISA small GTPase activation assay (Cytoskeleton cat# BK135), where levels of activated RhoA, Cdc42, and Rac1 were detected colorimetrically per manufacturer's instructions.

Single cell data collection: Sample collection and single cell sequencing was performed as previously described (57). Briefly, lung lobes were harvested, minced, and incubated for 30 minutes at 37°C in dissociation media (RPMI-1640 with 0.7 mg/ml collagenase XI and 30 mg/ml type IV bovine pancreatic DNase). After incubation, tissue was disassociated into a single-cell suspension by passage through a wide bore pipet tip and filtration through a 40 μm filter. The single-cell lung suspension was then counted, aliquoted, and blocked with CD-32 Fc block (BD cat # 553142) for 20 minutes on ice. After a 2% FBS staining buffer wash, cells were incubated with the conjugated primary antibodies anti-CD45 (BD cat # 559864) and anti-Ter119 (Biolegend cat# 116211). Samples from day 21 after LPS were also incubated with anti-CD326 antibody (BD cat # 563477) for epithelial enrichment.

scRNA-seq library preparation and next-generation sequencing: scRNA-seq libraries were generated using the Chromium Single Cell 5' library preparation kits (10X Genomics) following the manufacturer's recommendations and targeting 10,000 - 20,000 cells per sample. Sequencing was performed on an Illumina Novaseq 6000. CellRanger Count v3.1 (10X Genomics) was used to align reads onto the mm10 reference genome.

Analysis of single cell sequencing data: Ambient background RNA was cleaned from the scRNA-seq data with "SoupX"(58) as described previously (57) using the following genes to estimate the non-expressing cells, calculate the contamination fraction, and adjust the gene expression counts: *Dcn*, *Bgn*, *Aspn*, *Ecm2*, *Fos*, *Hbb-bs*, *Hbb-bt*, *Hba-a1*, *Hba-a2*, *Lyz1*, *Lyz2*, *Mgp*, *Postn*, *Scgb1a1*. For all datasets, quality filtering was then used to remove cells with > 15% or < 0.1% mitochondrial mRNA, and to remove cells with < 700 detected genes.

Dimensionality reduction, clustering, and visualization was performed using Seurat v4.0.5 and SCTransform v0.3.2.9008 with glmGamPoi v 1.6.0 (59-61). SCTransform was run with each sequencing run as a batch variable, and with the percentage of mitochondrial RNA as a regression variable. Further data cleaning was done to remove gene counts for *Gm42418*, which is likely a rRNA (62). Epithelial cells (*i.e. Epcam*+ cell clusters) were sorted *in silico* for downstream analysis. Epithelial cells were annotated with manual inspection of the following marker genes: *Epcam*, *Sftpa1*, *Sftpc*, *Hopx*, *Aqp5*, *Col4a3*, *Ager*, *Foxj1*, *Dynlrb2*, *Mki67*, *Scgb1a1*, *Scgb3a2*, *Cdkn1a*, *Cldn4*, *Ascl1*, and *Scg5*. All charts and heatmaps as part of the scRNAseq analysis were generated with ggplot2, and all parts of the analysis were run in R 4.1.1.

Data integration was performed using a previously published dataset (12). Reads were downloaded from the Gene Expression Omnibus (GSE113049) and processed using CellRanger Count v3.1 with the mm10 genome, followed by dimensionality reduction, clustering, and visualization as described above. Data were integrated with non-SoupX processed data using the 'IntegrateData' function in Seurat, following the workflow for data normalized with SCTransform. Samples from all experiments were combined, and clusters were annotated using marker genes described in the initial publication (12), and other canonical marker genes.

Cell label transfer was also utilized with a second published dataset (11). The annotated data matrix (h5ad file) was accessed as directed in the analysis code published as part of the methods (11). The raw counts from this annotated dataset were then processed using the Seurat workflow

described above, while maintaining the published cell annotations. The Seurat "TransferData" function was then used to transfer the cell annotations onto the dataset generated here.

A complete collection of all package versions, and code for all steps of the analysis is available at https://github.com/SucreLab. All sequencing data have been deposited to the NCBI GEO database; the reviewer link is available upon request.

Statistics: Comparison between two groups was performed by two-tailed t-test and 4-way comparison was done by one-way ANOVA. Individual *p*-values, t-values, F values, degrees of freedom, and sample size for each group is included in the figure legends and provided in **Supp. Table 1**. ScRNA-sequencing analysis was completed as above.

Study approval: All animal experiments were approved by the Institutional Animal Care and Use Committee at Vanderbilt University Medical Center.

Author contributions: EJP conceived the study, performed in vivo experiments, histological analysis, image analysis, interpreted the data, and wrote the manuscript. JMSS interpreted the scRNA-sequencing data and wrote the manuscript. FB, JG, JTB, and KTF performed histological analysis. PMG performed in vivo experiments, histological analysis, and protein assays. XD and SK performed protein assays. WH, CSJ performed in vivo experiments. JAK, NMN, and YL analyzed the scRNA-sequencing data. SHG assisted in manuscript preparation. RZ and TSB conceived of the study, interpreted the data, and wrote the manuscript.

Acknowledgements: The authors would like to thank Matt Tyska and Christopher V.E. Wright for content expertise and Brittany Matlock, Angela Jones, Kari Seedle, Caitlin McCormick, and David Nichols for technical assistance. This work was supported by NIH grants K08 HL127102 (EJP), R03 HL 154287 (EJP), R01 HL163195 (EJP), K08 HL143051 (JMSS), P01 HL092870 (TSB), R01 HL151016 (TSB), R01 DK069921 (RZ), R01 DK127589 (RZ), R01 DK088327 (RZ), R01 HL157373 (JTB), R01 HL150617 (SHG), R01 HL153246 (JAK), R38 HL143619 (trainee: KTF), Merit Review Grant 2 I01 BX002378 (TSB), I01 BX002196 (RZ), the Parker B. Francis Family Foundation (JMSS, JJG), American Society of Nephrology Ben J. Lipps Research Fellowship (FB), and the Vanderbilt Faculty Research Scholars award (JJG). Experiments were performed utilizing the Vanderbilt Cell Imaging Shared Resource (supported by NIH grants CA68485, DK20593, DK58404, DK59637, and EY08126). ScRNA-sequencing experiments were performed using the Vanderbilt Technologies for Advanced Genomics Core facility. Flow cytometry experiments were performed in the VUMC Flow Cytometry Shared Resource (supported by the Vanderbilt Ingram Cancer Center P30 CA68485 and the Vanderbilt Digestive Disease Research Center DK058404).

References

1. Mizikova I, and Morty RE. The Extracellular Matrix in Bronchopulmonary Dysplasia: Target and Source. *Front Med (Lausanne).* 2015;2:91.
2. Sokocevic D, Bonenfant NR, Wagner DE, Borg ZD, Lathrop MJ, Lam YW, et al. The effect of age and emphysematous and fibrotic injury on the re-cellularization of de-cellularized lungs. *Biomaterials.* 2013;34(13):3256-69.
3. Liang Q, Lin Q, Li Y, Luo W, Huang X, Jiang Y, et al. Effect of SIS3 on Extracellular Matrix Remodeling and Repair in a Lipopolysaccharide-Induced ARDS Rat Model. *J Immunol Res.* 2020;2020:6644687.
4. Roychaudhuri R, Hergrueter AH, Polverino F, Laucho-Contreras ME, Gupta K, Borregaard N, et al. ADAM9 is a novel product of polymorphonuclear neutrophils: regulation of expression and contributions to extracellular matrix protein degradation during acute lung injury. *J Immunol.* 2014;193(5):2469-82.
5. Humphrey JD, Dufresne ER, and Schwartz MA. Mechanotransduction and extracellular matrix homeostasis. *Nat Rev Mol Cell Biol.* 2014;15(12):802-12.
6. Hynes RO. Integrins: bidirectional, allosteric signaling machines. *Cell.* 2002;110(6):673-87.
7. Sun Z, Guo SS, and Fassler R. Integrin-mediated mechanotransduction. *J Cell Biol.* 2016;215(4):445-56.
8. Plosa EJ, Young LR, Gulleman PM, Polosukhin VV, Zaynagetdinov R, Benjamin JT, et al. Epithelial beta1 integrin is required for lung branching morphogenesis and alveolarization. *Development.* 2014;141(24):4751-62.

9. Plosa EJ, Benjamin JT, Sucre JM, Gulleman PM, Gleaves LA, Han W, et al. beta1 Integrin regulates adult lung alveolar epithelial cell inflammation. *JCI Insight.* 2020;5(2).

10. Negretti NM, Plosa EJ, Benjamin JT, Schuler BA, Habermann AC, Jetter CS, et al. A single-cell atlas of mouse lung development. *Development.* 2021;148(24).

11. Strunz M, Simon LM, Ansari M, Kathiriya JJ, Angelidis I, Mayr CH, et al. Alveolar regeneration through a Krt8+ transitional stem cell state that persists in human lung fibrosis. *Nat Commun.* 2020;11(1):3559.

12. Riemondy KA, Jansing NL, Jiang P, Redente EF, Gillen AE, Fu R, et al. Single cell RNA sequencing identifies TGFbeta as a key regenerative cue following LPS-induced lung injury. *JCI Insight.* 2019;5.

13. Zacharias WJ, Frank DB, Zepp JA, Morley MP, Alkhaleel FA, Kong J, et al. Regeneration of the lung alveolus by an evolutionarily conserved epithelial progenitor. *Nature.* 2018;555(7695):251-5.

14. Desai TJ, Brownfield DG, and Krasnow MA. Alveolar progenitor and stem cells in lung development, renewal and cancer. *Nature.* 2014;507(7491):190-4.

15. Nabhan AN, Brownfield DG, Harbury PB, Krasnow MA, and Desai TJ. Single-cell Wnt signaling niches maintain stemness of alveolar type 2 cells. *Science.* 2018;359(6380):1118-23.

16. Basil MC, Katzen J, Engler AE, Guo M, Herriges MJ, Kathiriya JJ, et al. The Cellular and Physiological Basis for Lung Repair and Regeneration: Past, Present, and Future. *Cell Stem Cell.* 2020;26(4):482-502.

17. Juul NH, Stockman CA, and Desai TJ. Niche Cells and Signals that Regulate Lung Alveolar Stem Cells In Vivo. *Cold Spring Harb Perspect Biol.* 2020;12(12).

18. Paris AJ, Hayer KE, Oved JH, Avgousti DC, Toulmin SA, Zepp JA, et al. STAT3-BDNF-TrkB signalling promotes alveolar epithelial regeneration after lung injury. *Nat Cell Biol.* 2020;22(10):1197-210.

19. Yuan T, Klinkhammer K, Lyu H, Gao S, Yuan J, Hopkins S, et al. Temporospatial Expression of Fgfr1 and 2 During Lung Development, Homeostasis, and Regeneration. *Front Pharmacol.* 2020;11:120.

20. Zhou B, Flodby P, Luo J, Castillo DR, Liu Y, Yu FX, et al. Claudin-18-mediated YAP activity regulates lung stem and progenitor cell homeostasis and tumorigenesis. *J Clin Invest.* 2018;128(3):970-84.

21. Choi J, Park JE, Tsagkogeorga G, Yanagita M, Koo BK, Han N, et al. Inflammatory Signals Induce AT2 Cell-Derived Damage-Associated Transient Progenitors that Mediate Alveolar Regeneration. *Cell Stem Cell.* 2020;27(3):366-82 e7.

22. Kobayashi Y, Tata A, Konkimalla A, Katsura H, Lee RF, Ou J, et al. Persistence of a regeneration-associated, transitional alveolar epithelial cell state in pulmonary fibrosis. *Nat Cell Biol.* 2020;22(8):934-46.

23. Haake SM, Plosa EJ, Kropski JA, Venton LA, Reddy A, Bock F, et al. Ligand-independent integrin beta1 signaling supports lung adenocarcinoma development. *JCI Insight.* 2022;7(15).

24. Perl AK, Zhang L, and Whitsett JA. Conditional expression of genes in the respiratory epithelium in transgenic mice: cautionary notes and toward building a better mouse trap. *Am J Respir Cell Mol Biol.* 2009;40(1):1-3.

25. Saxon JA, Cheng DS, Han W, Polosukhin VV, McLoed AG, Richmond BW, et al. p52 Overexpression Increases Epithelial Apoptosis, Enhances Lung Injury, and Reduces Survival after Lipopolysaccharide Treatment. *J Immunol.* 2016;196(4):1891-9.

26. Lake BB, Codeluppi S, Yung YC, Gao D, Chun J, Kharchenko PV, et al. A comparative strategy for single-nucleus and single-cell transcriptomes confirms accuracy in predicted cell-type expression from nuclear RNA. *Sci Rep.* 2017;7(1):6031.

27. Fischer BM, Pavlisko E, and Voynow JA. Pathogenic triad in COPD: oxidative stress, protease-antiprotease imbalance, and inflammation. *Int J Chron Obstruct Pulmon Dis.* 2011;6:413-21.

28. Kaur G, and Batra S. Regulation of DNA methylation signatures on NF-kappaB and STAT3 pathway genes and TET activity in cigarette smoke extract-challenged cells/COPD exacerbation model in vitro. *Cell Biol Toxicol.* 2020;36(5):459-80.

29. Li J, Wang Z, Chu Q, Jiang K, Li J, and Tang N. The Strength of Mechanical Forces Determines the Differentiation of Alveolar Epithelial Cells. *Dev Cell.* 2018;44(3):297-312 e5.

30. Nobes CD, and Hall A. Rho, rac, and cdc42 GTPases regulate the assembly of multimolecular focal complexes associated with actin stress fibers, lamellipodia, and filopodia. *Cell.* 1995;81(1):53-62.

31. Takashimizu Y, and Iiyoshi M. New parameter of roundness R: circularity corrected by aspect ratio. *Progress in Earth and Planetary Science.* 2016;3(1):2.

32. Rannels DE, and Rannels SR. Influence of the extracellular matrix on type 2 cell differentiation. *Chest.* 1989;96(1):165-73.

33. Zhou Y, Horowitz JC, Naba A, Ambalavanan N, Atabai K, Balestrini J, et al. Extracellular matrix in lung development, homeostasis and disease. *Matrix Biol.* 2018;73:77-104.

34. Jandl K, Mutgan AC, Eller K, Schaefer L, and Kwapiszewska G. The basement membrane in the cross-roads between the lung and kidney. *Matrix Biol.* 2022;105:31-52.

35. Zhang F, Fan D, and Mo XN. Prohibitin and the extracellular matrix are upregulated in murine alveolar epithelial cells with LPSinduced acute injury. *Mol Med Rep.* 2018;17(6):7769-73.

36. Rawlins EL. Lung epithelial progenitor cells: lessons from development. *Proceedings of the American Thoracic Society.* 2008;5(6):675-81.

37. Liberti DC, Kremp MM, Liberti WA, 3rd, Penkala IJ, Li S, Zhou S, et al. Alveolar epithelial cell fate is maintained in a spatially restricted manner to promote lung regeneration after acute injury. *Cell Rep.* 2021;35(6):109092.

38. Xu C, Li X, Topham MK, and Kuwada SK. Regulation of sonic hedgehog expression by integrin beta1 and epidermal growth factor receptor in intestinal epithelium. *IUBMB Life.* 2014;66(10):694-703.

39. Santa-Cruz Mateos C, Valencia-Exposito A, Palacios IM, and Martin-Bermudo MD. Integrins regulate epithelial cell shape by controlling the architecture and mechanical properties of basal actomyosin networks. *PLoS Genet.* 2020;16(6):e1008717.

40. Dominguez-Gimenez P, Brown NH, and Martin-Bermudo MD. Integrin-ECM interactions regulate the changes in cell shape driving the morphogenesis of the Drosophila wing epithelium. *J Cell Sci.* 2007;120(Pt 6):1061-71.

41. Randles MJ, Lausecker F, Humphries JD, Byron A, Clark SJ, Miner JH, et al. Basement membrane ligands initiate distinct signalling networks to direct cell shape. *Matrix Biol.* 2020;90:61-78.

42. Ron A, Azeloglu EU, Calizo RC, Hu M, Bhattacharya S, Chen Y, et al. Cell shape information is transduced through tension-independent mechanisms. *Nat Commun.* 2017;8(1):2145.

43. Hunter MP, and Zegers MM. Pak1 regulates branching morphogenesis in 3D MDCK cell culture by a PIX and beta1-integrin-dependent mechanism. *Am J Physiol Cell Physiol.* 2010;299(1):C21-32.

44. Muller PM, Rademacher J, Bagshaw RD, Wortmann C, Barth C, van Unen J, et al. Systems analysis of RhoGEF and RhoGAP regulatory proteins reveals spatially organized RAC1 signalling from integrin adhesions. *Nat Cell Biol.* 2020;22(4):498-511.

45. Rivas M, Gupta G, Costanzo L, Ahmed H, Wyman AE, and Geraghty P. Senescence: Pathogenic Driver in Chronic Obstructive Pulmonary Disease. *Medicina (Kaunas).* 2022;58(6).

46. MacNee W. Is Chronic Obstructive Pulmonary Disease an Accelerated Aging Disease? *Ann Am Thorac Soc.* 2016;13 Suppl 5:S429-S37.

47. Brass DM, Hollingsworth JW, Cinque M, Li Z, Potts E, Toloza E, et al. Chronic LPS inhalation causes emphysema-like changes in mouse lung that are associated with apoptosis. *Am J Respir Cell Mol Biol.* 2008;39(5):584-90.

48. Ghorani V, Boskabady MH, Khazdair MR, and Kianmeher M. Experimental animal models for COPD: a methodological review. *Tob Induc Dis.* 2017;15:25.

49. Ishii T, Hosoki K, Nikura Y, Yamashita N, Nagase T, and Yamashita N. IFN Regulatory Factor 3 Potentiates Emphysematous Aggravation by Lipopolysaccharide. *J Immunol.* 2017;198(9):3637-49.

50. Shu J, Lu W, Yang K, Zheng Q, Li D, Li Y, et al. Establishment and evaluation of chronic obstructive pulmonary disease model by chronic exposure to motor vehicle exhaust combined with lipopolysaccharide instillation. *Exp Physiol.* 2018;103(11):1532-42.

51. Singla E, Puri G, Dharwal V, and Naura AS. Gallic acid ameliorates COPD-associated exacerbation in mice. *Mol Cell Biochem.* 2021;476(1):293-302.

52. Wright JL, and Churg A. Animal models of COPD: Barriers, successes, and challenges. *Pulm Pharmacol Ther.* 2008;21(5):696-8.

53. Perl AK, Tichelaar JW, and Whitsett JA. Conditional gene expression in the respiratory epithelium of the mouse. *Transgenic Res.* 2002;11(1):21-9.

54. Raghavan S, Bauer C, Mundschau G, Li Q, and Fuchs E. Conditional ablation of beta1 integrin in skin. Severe defects in epidermal proliferation, basement membrane formation, and hair follicle invagination. *J Cell Biol.* 2000;150(5):1149-60.

55. Rice WR, Conkright JJ, Na CL, Ikegami M, Shannon JM, and Weaver TE. Maintenance of the mouse type II cell phenotype in vitro. *Am J Physiol Lung Cell Mol Physiol.* 2002;283(2):L256-64.

56. Young LR, Gulleman PM, Bridges JP, Weaver TE, Deutsch GH, Blackwell TS, et al. The alveolar epithelium determines susceptibility to lung fibrosis in Hermansky-Pudlak syndrome. *Am J Respir Crit Care Med.* 2012;186(10):1014-24.

57. Schuler BA, Habermann AC, Plosa EJ, Taylor CJ, Jetter C, Negretti NM, et al. Age-determined expression of priming protease TMPRSS2 and localization of SARS-CoV-2 in lung epithelium. *J Clin Invest.* 2021;131(1).

58. Young MD, Behjati S. . SoupX removes ambient RNA contamination from droplet based single-cell RNA sequencing data. *bioRxiv.* 2020;303727.

59. Hao Y, Hao S, Andersen-Nissen E, Mauck WM, 3rd, Zheng S, Butler A, et al. Integrated analysis of multimodal single-cell data. *Cell.* 2021;184(13):3573-87 e29.

60. Hafemeister C, and Satija R. Normalization and variance stabilization of single-cell RNA-seq data using regularized negative binomial regression. *Genome Biol.* 2019;20(1):296.

61. Ahlmann-Eltze C, and Huber W. glmGamPoi: fitting Gamma-Poisson generalized linear models on single cell count data. *Bioinformatics.* 2021;36(24):5701-2.

62. Kimmel JC, Hwang AB, Scaramozza A, Marshall WF, and Brack AS. Aging induces aberrant state transition kinetics in murine muscle stem cells. *Development.* 2020;147(9).

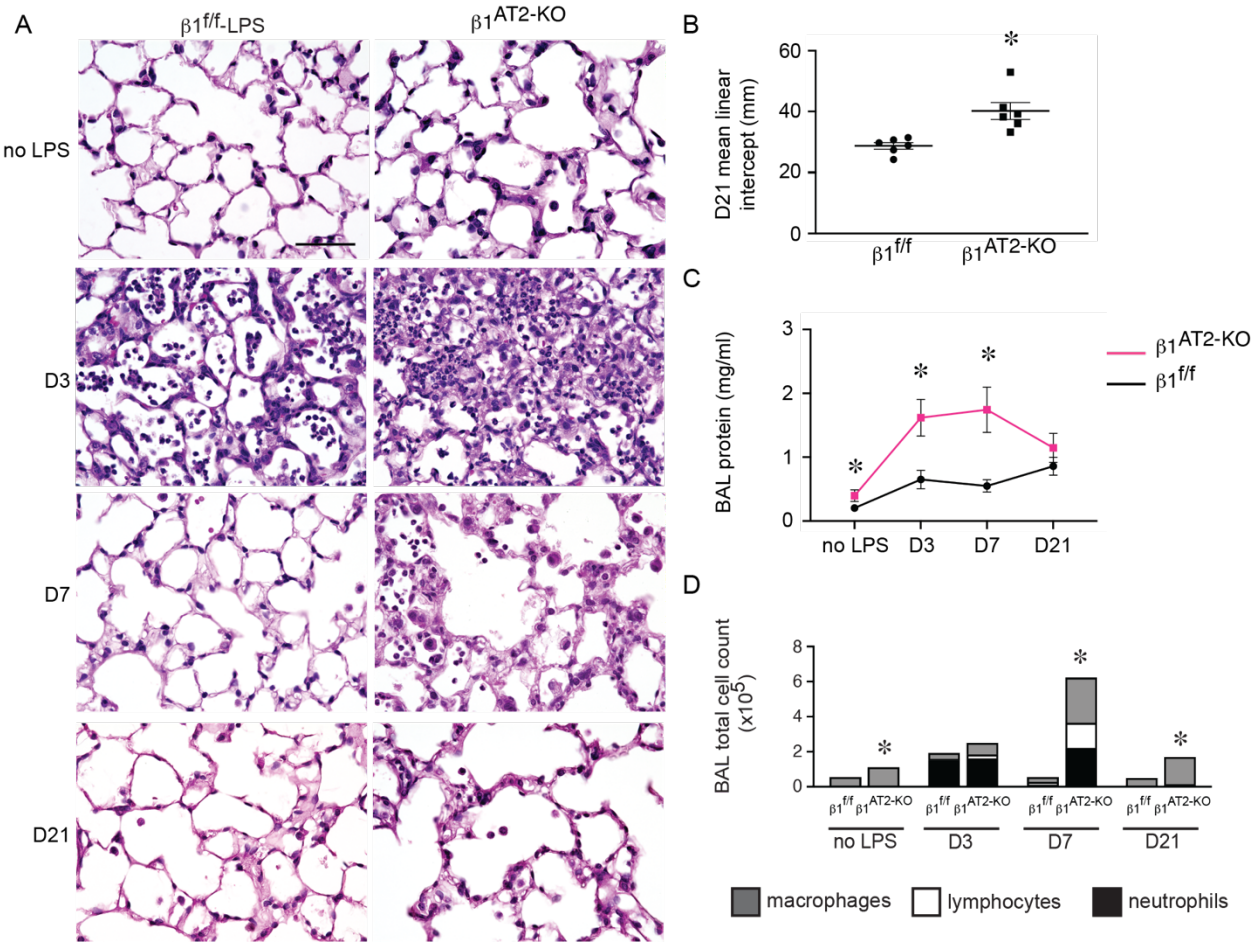

Figure 1. β1 integrin deletion in AT2s results in increased inflammation, abnormal repair, and decreased survival after LPS-induced injury. (A) Representative images of lung histology demonstrate increased edema at 3 and 7 days post-injury in $\beta1^{AT2\text{-}KO}$ lungs compared to $\beta1^{f/f}$ lungs, as well as persistent inflammation and emphysematous remodeling in $\beta1^{AT2\text{-}KO}$ lungs by 21 days post-LPS. -LPS refers to uninjured mice; D3, D7, and D21 refer to 3, 7, and 21 days post-LPS injury, respectively. (B) Mean linear intercept quantified emphysematous alveolar remodeling at 21 days post-LPS, 28.5±0.9 μm in $\beta1^{f/f}$ lungs vs. 40.2±2.8 μm in $\beta1^{AT2\text{-}KO}$ lungs (n=6-7 mice/ group, p=0.0014 by two-tailed t-test). (C) Bicinchoninic Acid protein assay quantified increased bronchoalveolar lavage (BAL) fluid protein in uninjured $\beta1^{AT2\text{-}KO}$ lungs and at 3 and 7 days post-LPS injury in $\beta1^{AT2\text{-}KO}$ lungs compared to $\beta1^{f/f}$ lungs at the same time points (n=6-14 mice/ group, two-tailed t-test comparing genotypes at each time point, p=0.0485 for uninjured mice; p=0.0036 at D3; p=0.005 at D7; p=0.2628 at D21). (D) BAL cell counts are significantly increased in $\beta1^{AT2\text{-}KO}$ lungs compared to $\beta1^{f/f}$ littermates in uninjured mice and at 7 and 21 days post-LPS. Peak inflammation is present at 7 days in $\beta1^{AT2\text{-}KO}$ lungs, 55,663±3306 cells/ ml in $\beta1^{f/f}$ BALF versus 624,000±118,753 cells/ml in $\beta1^{AT2\text{-}KO}$ BAL (n=6-26 mice/group, two-tailed t-test comparing genotypes at each time point, p=0.0002 for uninjured mice; p=0.0730 at D3; p=0.0007 at D7; p<0.0001 at D21). Total numbers of BALF macrophages are significantly increased in uninjured $\beta1^{AT2\text{-}KO}$ mice and at day 7 and day 21, lymphocytes and neutrophils are significantly increased in $\beta1^{AT2\text{-}KO}$ BAL at day 7 only. Scale bar=50 μm for (A). ∗ $p < 0.05$

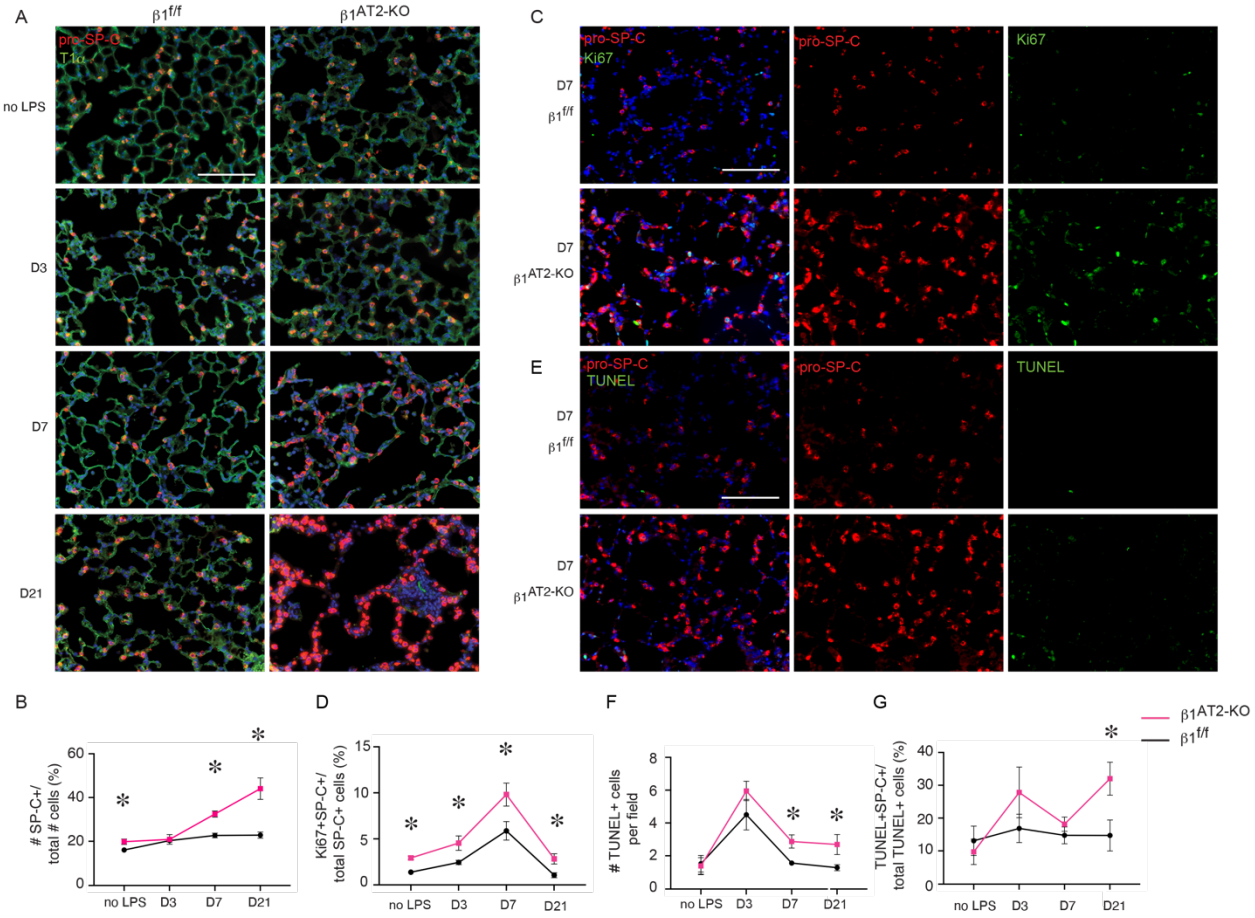

Figure 2. β1-deficient AT2 cells increase in number post-LPS injury. (A) Lung sections immunostained for pro-SP-C (red) and T1α (green) demonstrate increased AT2 cells and decreased T1α in $\beta1^{AT2\text{-}KO}$ lungs by day 7 post-injury. (B) Quantification by percentage of number pro-SP-C+ cells per total cells (n=6-8 mice/ group; 5 sections per mouse; p=0.0247 for uninjured (-LPS) mice; p=0.8220 at D3; p=0.0001 at D7; p=0.0009 at D21). (C) Immunodetection of the proliferation marker Ki67 (green) and pro-SP-C (red) show peak proliferation of AT2s in $\beta1^{AT2\text{-}KO}$ lungs at day 7 as merged or single-channel panels. (D) Quantification of proliferating AT2 cells by percentage of total pro-SP-C+ AT2s (n=6-8 mice/ group, 10 sections/ mouse; p=0.0003 for uninjured mice; p=0.0311 at D3; p=0.0310 at D7; p=0.0128 at D21). (E) TUNEL/ pro-SP-C immunodetection demonstrates low levels of apoptotic AT2s at D7 in $\beta1^{AT2\text{-}KO}$ lungs. (F) Quantification of total TUNEL+ cells per field shows a small but significant increase in apoptotic cells at D7 and D21 (n=6-18 mice/ group, 10 sections/ mouse; p=0.8596 for uninjured mice; p=0.2184 at D3; p=0.0011 at D7; p=0.0439 at D21). (G) Quantification of TUNEL/pro-SP-C dual + cells per total number TUNEL+ cells shows a modest increase in apoptotic AT2 cells at day 21 (n=6-18 mice/ group, 10 sections/ mouse; p=0.5867 for uninjured mice; p=0.2436 at D3; p=0.3688 at D7; p=0.0246 at D21). $* p <$ 0.05. Scale bar = 100 μm for A, C, and E. Two-tailed t-test was used to compare genotypes at each time point for B, D, F, and G.

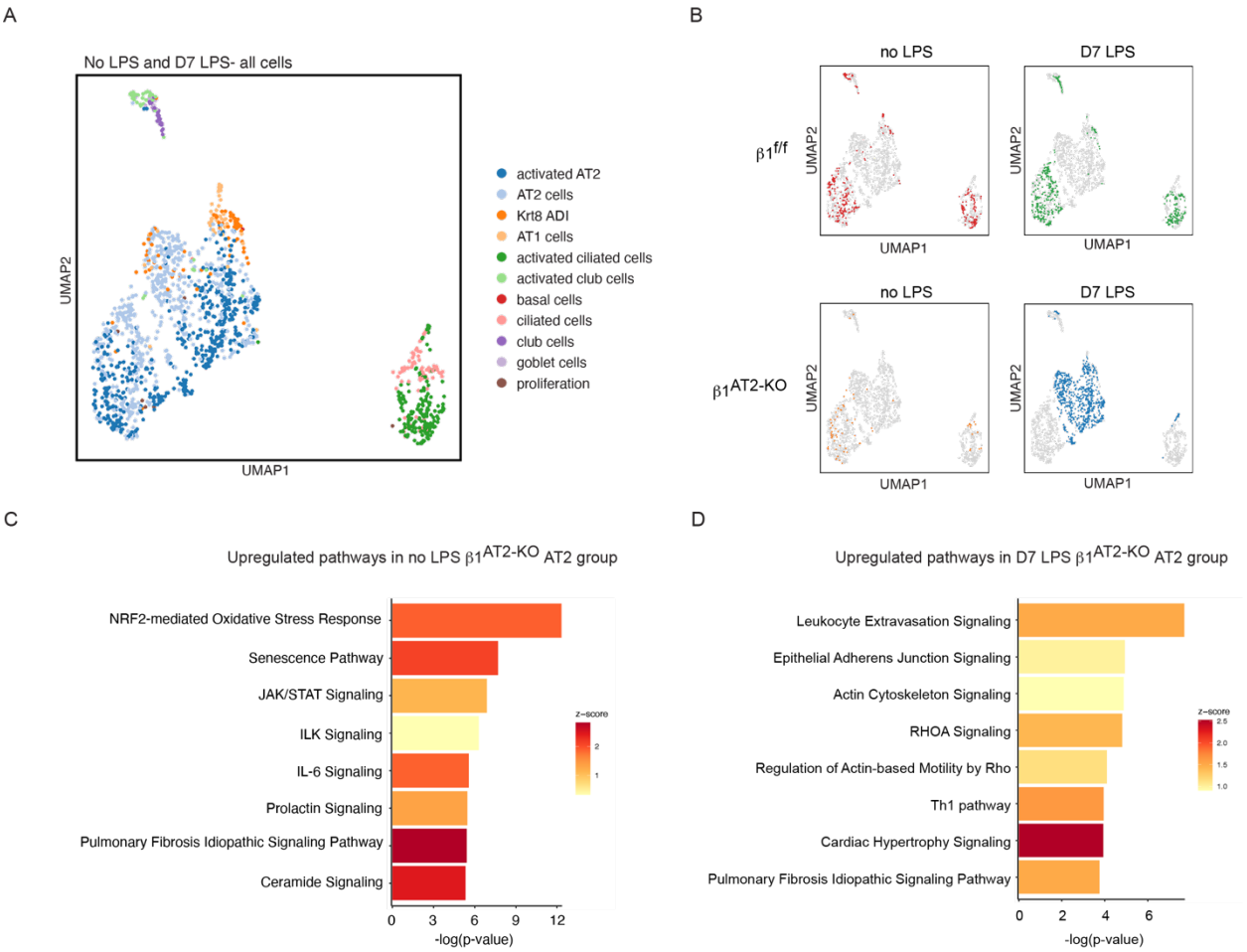

Figure 3. Overabundant AT2s are transcriptionally distinct during repair in β1$^{AT2\text{-}KO}$ mice. (A) UMAP of all epithelial cells from β1$^{f/f}$ and β1$^{AT2\text{-}KO}$ lungs ± LPS clustered by label transfer from Strunz et al (11). (B) Individual epithelial populations by group reveal transcriptionally distinct AT2s and activated AT2s in day 7 LPS-treated β1$^{AT2\text{-}KO}$ lungs. (C) Ingenuity Pathway Analysis on combined AT2 groups from unimjured β1$^{f/f}$ and β1$^{AT2\text{-}KO}$ lungs demonstrate upregulation of oxidative stress, senescence, and inflammatory pathways in β1$^{AT2\text{-}KO}$ lungs. (D) Ingenuity Pathway Analysis shows upregulation of actin cytoskeleton signaling pathways at seven days after LPS treatment.

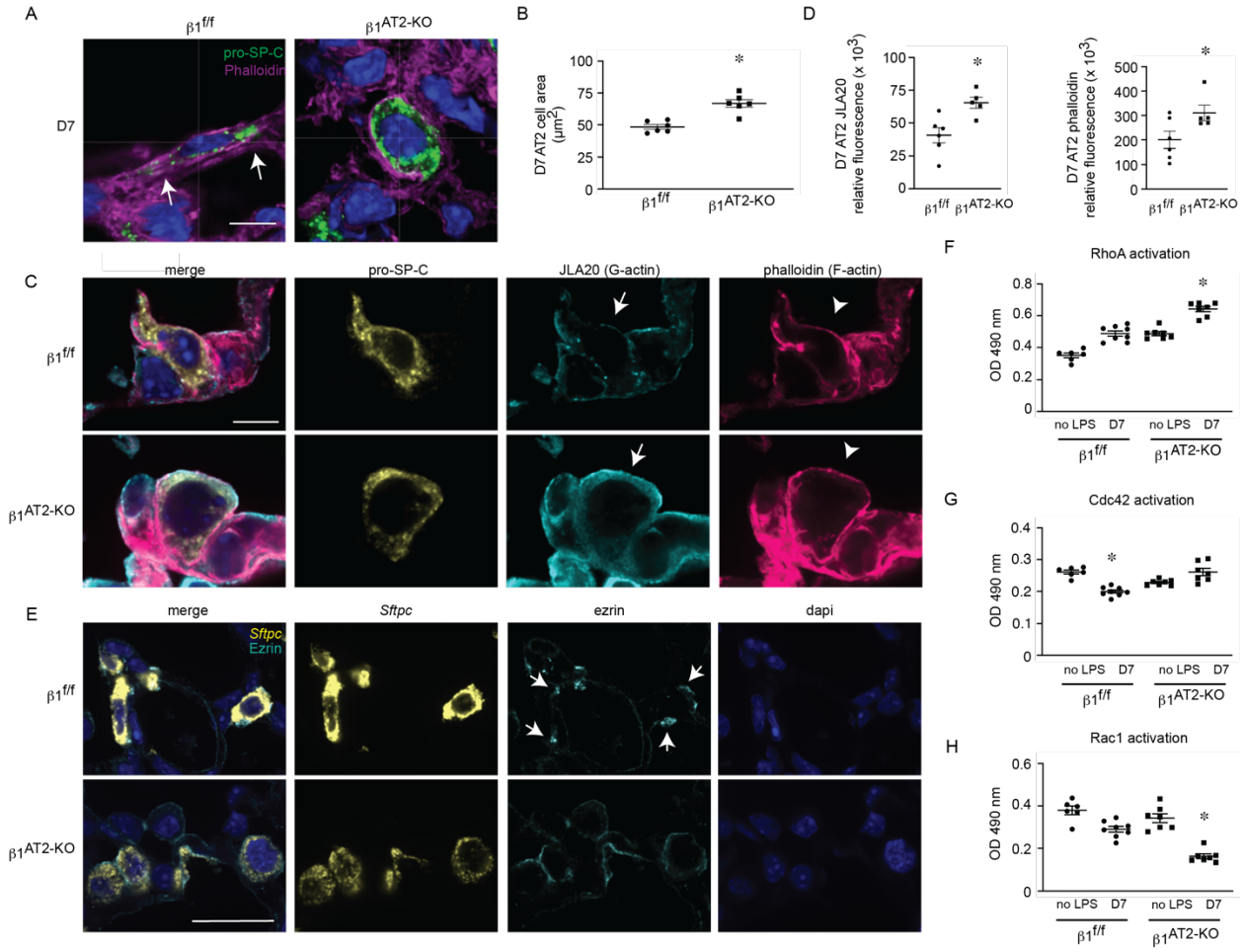

Figure 4. β1 integrin regulates actin localization and RhoA GTPase activation during alveolar repair. (A) High-power images of thick frozen sections from day 7 LPS-treated $\beta1^{f/f}$ and $\beta1^{AT2\text{-}KO}$ lungs immunostained for pro-SP-C (green) with phalloidin F-actin probe (magenta), arrows indicate areas of actin-rich lateral protrusions. (B) Area of pro-SP-C+ AT2 cells from day 7 LPS-treated $\beta1^{f/f}$ and $\beta1^{AT2\text{-}KO}$ mice (48.4±1.8 μm^2 in $\beta1^{f/f}$ lungs compared to 66.8±3.0 μm^2 in $\beta1^{AT2\text{-}KO}$ lungs, n = 6 mice/group, ≥ 40 cells measured/ mouse imaged from 3 different sections, two-tailed t-test, p=0.0004). (C) High-power images of frozen sections prepared from day 7 injured $\beta1^{f/f}$ and $\beta1^{AT2\text{-}KO}$ lungs immunostained for pro-SP-C with JLA20 and phalloidin probes applied to detect G-actin and F-actin, respectively. Membrane localization of G-actin denoted by arrows and F-actin by arrowheads. (D) Quantification of JLA20 and phalloidin expression in pro-SP-C+ AT2 cells in $\beta1^{f/f}$ and $\beta1^{AT2\text{-}KO}$ lungs 7 days after LPS (n = 5-6 mice/ group, 10 sections/ mouse, two-tailed t-test with p=0.0088 for JLA20 and p=0.0482 for phalloidin). (E) Representative high-power images from day 7 LPS-treated $\beta1^{f/f}$ and $\beta1^{AT2\text{-}KO}$ lungs immunostained for ezrin (cyan) with AT2 cells identified by RNA *in situ* hybridization for *Sftpc* (yellow). Arrows indicate ezrin expression localized to lateral extensions in $\beta1^{f/f}$ AT2 cells, whereas diffuse, non-focal ezrin expression along the cell membrane is seen in $\beta1^{AT2\text{-}KO}$ AT2 cells. (F-H) GTPase activation assay performed on AT2 cell lysates collected from uninjured and day 7 LPS-treated $\beta1^{f/f}$ and $\beta1^{AT2\text{-}KO}$ lungs (n=6-8 mice/ group for each assay; RhoA one-way ANOVA p<0.0001, F value 53.42, df=3; Cdc42 one-way ANOVA p<0.001, F value 17.46, df=3; Rac1 one-way ANOVA p<0.0001, F value 31.09, df=3). ∗ $p < 0.05$. Scale bar = 5 μm for A and C, 25 μm for panels in E.

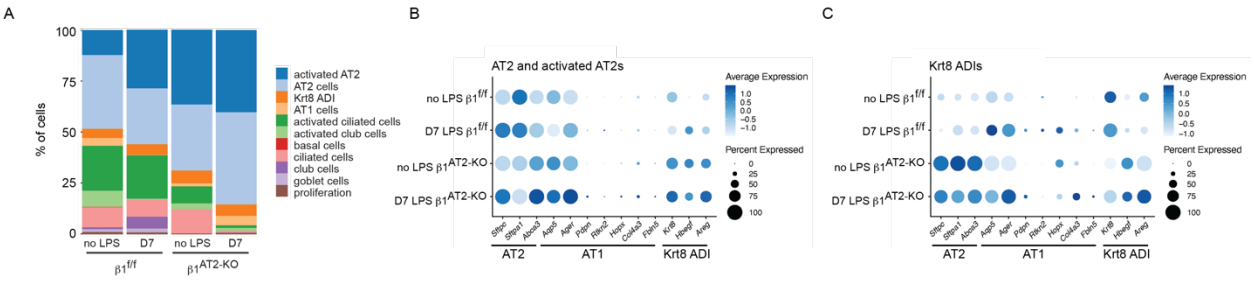

Figure 5. Post-injury β1 deficient AT2s exhibit an AT2-AT1 mixed epithelial transcriptomic phenotype. (A) Stacked bar graph of epithelial proportions demonstrates an expansion of the AT2 and activated AT2 populations in day 7 LPS-treated $\beta1^{AT2\text{-}KO}$ lungs. (B-C) Marker gene expression by genotype and treatment group in AT2/ activated AT2 and Krt8+ ADI clusters, in which higher expression is represented with a darker color and the size of the dot reflects the proportion of cells expressing that marker.

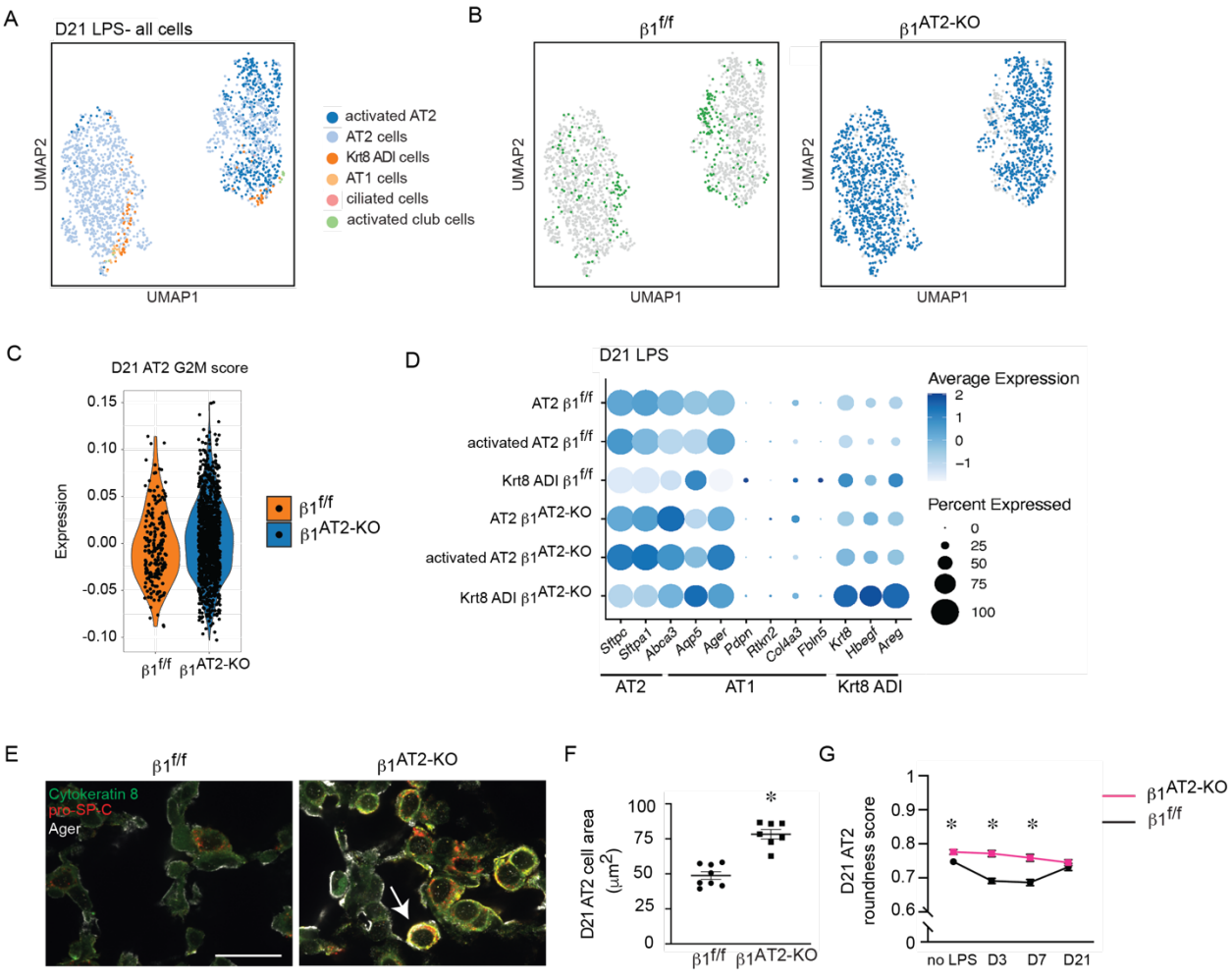

Figure 6. AT2s of mixed transcriptomic phenotype persist, proliferate, and maintain an enlarged, rounded cell shape in late alveolar repair. (A) UMAP of all epithelial cells from $\beta1^{f/f}$ and $\beta1^{AT2\text{-}KO}$ lungs 21 days after LPS treatment clustered by label transfer from Strunz et al (11). (B) Individual epithelial populations by group reveal transcriptionally abundant AT2s and activated AT2s in day 21 LPS-treated $\beta1^{AT2\text{-}KO}$ lungs. (C) G2M proliferation score demonstrates sustained AT2 proliferation at 21 days after LPS injury in $\beta1^{AT2\text{-}KO}$ lungs. (D) Marker gene expression by genotype in AT2, activated AT2, and Krt8 ADI clusters, in which higher expression is represented with a darker color and the size of the dot reflects the proportion of cells expressing that marker. (E) Representative high-power images of $\beta1^{f/f}$ and $\beta1^{AT2\text{-}KO}$ lungs 21 days after LPS co-immunostained for pro-SP-C, cytokeratin 8, and Ager. Arrow denotes occasional rounded cells co-expressing AT2, intermediate cell, and AT1 markers. (F) Area of pro-SP-C+ AT2 cells from day 21 LPS-treated $\beta1^{f/f}$ and $\beta1^{AT2\text{-}KO}$ mice (48.8±2.8 μm^2 in $\beta1^{f/f}$ lungs compared to 78.3±3.3 μm^2 in $\beta1^{AT2\text{-}KO}$ lungs, ≥ 35 cells measured/ mouse imaged from 3 different sections, n = 7-8 mice/ group, two-tailed t-test with $p<0.0001$). (G) Roundness score calculated from pro-SP-C+ cells from uninjured, day 3, day 7, and day 21 LPS-treated $\beta1^{f/f}$ and $\beta1^{AT2\text{-}KO}$ mice (≥ 35 cells measured/ mouse from at least 3 different sections, n=6-8 mice/ group, two-tailed t-test comparing genotypes at each time point, $p=0.0222$ for uninjured mice; $p<0.0001$ at D3; $p=0.0003$ at D7; $p=0.3641$ at D21). ∗ $p < 0.05$. Scale bar = 25 μm.